

Controlling Fragment Competition on Pathways to Addressable Self-Assembly

Jim Madge,[†] David Bourne,[‡] and Mark A. Miller^{*,†}

[†]*Department of Chemistry, Durham University, South Road, Durham DH1 3LE, United Kingdom*

[‡]*Department of Mathematical Sciences, Durham University, South Road, Durham DH1 3LE, United Kingdom*

E-mail: m.a.miller@durham.ac.uk

Phone: +44 (0)191 3342037

Abstract

Addressable self-assembly is the formation of a target structure from a set of unique molecular or colloidal building-blocks, each of which occupies a defined location in the target. The requirement that each type of building-block appears exactly once in each copy of the target introduces severe restrictions on the combinations of particles and on the pathways that lead to successful self-assembly. These restrictions can limit the efficiency of self-assembly and the final yield of the product. In particular, partially formed fragments may compete with each other if their compositions overlap, since they cannot be combined. Here, we introduce a “completability” algorithm to quantify competition between self-assembling fragments and use it to deduce general principles for suppressing the effects of fragment incompatibility in the self-assembly of small addressable clusters. Competition originates from loops in the bonding network of the target structure, but loops may be needed to provide structural rigidity and thermodynamic stability. An optimal compromise can be achieved by careful choice of bonding networks and by promoting semi-hierarchical pathways that rule out competition between early fragments. These concepts are illustrated in simulations of self-assembly in two contrasting addressable targets of 20 unique components each.

Introduction

Self-assembly describes a broad class of processes, both naturally occurring and human-made. In all cases, an ordered structure forms spontaneously and with high fidelity from an initially disordered system of molecular or colloidal building-blocks. Increasingly detailed control is now being exerted over target structures and assembly pathways by the use of sophisticated building-blocks such as patchy colloids,¹⁻³ and DNA.⁴

DNA is a powerful starting-point for self-assembly because the binding of complementary nucleotide sequences is so much stronger than that of sequences that do not match. Hence, different nucleotide sequences can be used to control the pairwise interactions between

building-blocks and thereby assemble structures from multiple components. This concept can be exploited by grafting DNA onto colloidal particles,⁵⁻⁷ by folding long DNA strands like origami,^{8,9} or by making tiles^{10,11} or bricks¹²⁻¹⁴ from short DNA helices. These DNA-based approaches have introduced the paradigm of addressable self-assembly,¹⁵ in which each component of a complex structure is unique and has a specified location.

Addressable assembly has the advantage of providing site-by-site control over the properties of the final structure. It also avoids the need to rely on symmetry, since building-blocks that are unique may each have environments that are also unique, making it possible to assemble structures of arbitrary complexity. In this sense, addressable assembly lies at the opposite extreme from some well-known examples of self-assembly such as virus capsids.¹⁶ In capsid assembly, the high symmetry of the protein shell (often icosahedral) provides a large number of equivalent or quasi-equivalent molecular environments, so that the shell can form from multiple copies of just one building-block in some cases.¹⁷

In a fully addressable structure, each type of building-block appears only once, and this constraint introduces some important new entropic considerations.^{15,18} Self-assembly of a target structure always requires a specific number N of building-blocks to come together. In a one-component system, any N available monomers are acceptable and they may appear in the structure in any order. In contrast, addressable assembly requires a specific combination of building-blocks (one of each type) and each has a particular location within the target. Hence, the number of acceptable particle permutations in the fully assembled system is greatly reduced in the addressable case, lowering the statistical weight of the assembled state. Likewise, the number and nature of pathways leading to correct assembly are dramatically altered. Two consequences of these characteristics are that addressable assembly is usually only viable within a narrow temperature window, and that the yield may be low.^{14,16,19,20}

Theoretical and computational work^{19,21-23} has shown that addressable assembly can be understood as a non-classical nucleation process. The existence of a nucleation free-energy barrier and a critical cluster assists correct assembly partly by slowing down the approach

to equilibrium and by providing the opportunity for incorrectly formed fragments to break up. A time-dependent temperature protocol can help assembly, starting with nucleation at a higher temperature and proceeding with growth at a lower temperature,^{20,21,24} even if the cooling schedule spans a very narrow range.¹⁴

A particular feature of addressable assembly is that correct fragments of the target can begin to form but then compete with each other because they have overlapping compositions that prevent them from combining or from all reaching completion. Assembly in a one-component system is less prone to this problem because any monomer may contribute to growth of a structure.¹⁶ This problem can be partly mitigated by the nucleation kinetics described above. Nevertheless, it should be possible to raise yields by positively avoiding competition between partially formed fragments.

With some notable exceptions,^{25–28} most computational work on addressable assembly has concentrated on the formation of just one copy of the target structure, starting from the perfect stoichiometry of only one building-block of each type. Hence, such studies do not explicitly account for fragment competition. Here, we focus directly on this intrinsic aspect of addressable assembly. We introduce a metric for quantifying fragment competition in terms of a “completeness index” that describes the instantaneous state of the system. This index helps to identify where competition is the limiting factor in self-assembly. We then show how competition can be reduced by certain choices for the topology and strength of the bonding network in the target structure. General principles emerge that allow higher yields to be reached, and that make assembly robust over a wider range of temperatures.

The rest of the article is structured as follows. We start by specifying a variant of an idealized coarse-grained model and a dynamics-like Monte Carlo (MC) method^{16,29} for studying addressable assembly. We then show how to quantify fragment competition by introducing the completeness index and algorithm. We use these tools to analyze the self-assembly of two contrasting target structures. Finally, we summarize the general principles and conclusions that can be extracted from the study.

Model

Patchy potential

In previous work, we introduced a generic off-lattice model to compare design strategies for self-assembly¹⁶ and to optimize the design of building-blocks with controllable complexity.²⁹ The building-blocks were hard cubes whose faces were patterned with attractive patches that drive the self-assembly. Here, we use a variant of the patchy cube model to focus on fragment competition. The key modifications are simplifying the patterned faces to a single interaction site per face, and placing the minimum of the pairwise attraction slightly away from contact between the hard cores to avoid artificially severe steric requirements in closely packed targets. Our model has much in common with the off-lattice version of a model studied by Jacobs, Oxtoby and Frenkel.³⁰

The patchy cubes have edges of length d . The cores are impenetrable and overlap detection is handled in the simulations by treating them as oriented bounding boxes.³¹⁻³³ Each face may have up to one attractive site. Pairwise interactions between these patches on different cubes are attenuated by both an angular and a torsional factor such that the minimum occurs when the interacting faces are parallel and the cubes have a particular mutual orientation with respect to the line that joins their centers. The angular attenuation causes each patch to be associated with a particular face of the building-block and captures the resulting directionality of the attractive interactions. The torsional contribution to the potential accounts for the overall effect of a more detailed description of the interactions³⁴ in terms of a pattern of interactions on each face of the cubes. Such patterns were previously represented explicitly when they were the main focus of an investigation.^{16,29}

The pairwise interaction is an attractive well that switches between a Morse potential and Gaussian repulsion at the minimum of the potential. The value, gradient and curvature of the two parts are matched at the point of hand-over. The functional form of the interaction

is

$$V_{ij}^M(r_{ij}) = \begin{cases} \varepsilon_{ij} [e^{-2\alpha(r_{ij}-5d/4)} - 2e^{-\alpha(r_{ij}-5d/4)}] & \text{if } r_{ij} > 5d/4 \\ \varepsilon_{ij} \exp(-\alpha^2[r_{ij} - 5d/4]^2) & \text{if } d < r_{ij} \leq 5d/4 \end{cases} \quad (1)$$

where r_{ij} is the distance between patches i and j . α is a parameter that controls the range of the potential, which we fix¹⁶ at $\alpha = 6d^{-1}$, which means that the curvature of the potential at its minimum is the same as that of the Lennard-Jones potential. ε_{ij} determines the depth of the potential at its minimum. For the addressable systems considered in this work, the identity of the building-blocks is effectively specified by the set of ε_{ij} values for all combinations of patches. Non-zero values of this parameter determine which faces of the different particles bind to each other and how strongly they do so.

The interaction site for each patch is embedded in the particle perpendicular to the face on which the patch sits at a depth of $d/2$ (Fig. 1). The distance dependence of the exponent in Eq. (1) therefore ensures that the minimum of the interaction between two patches occurs when two particles faces are separated by a distance of $d/4$. This separation helps ensure that the hard repulsion of particles does not artificially prevent dense clusters from forming. The potential is truncated at a distance of $2d$. To avoid a discontinuity at the cut-off, the potential is shifted by $V_{ij}^M(2d)$. The potential is then rescaled so that the value of the potential at the minimum is ε_{ij} .

The angular attenuation of the potential is a Gaussian of the form

$$V^{\text{ang}}(\hat{\mathbf{r}}_{ij}, \hat{\mathbf{u}}_i, \hat{\mathbf{u}}_j) = \exp\left(-\frac{\theta_i^2 + \theta_j^2}{2\sigma_{\text{ang}}^2}\right), \quad (2)$$

where $\hat{\mathbf{r}}_{ij}$ is the unit vector from patch i to patch j (Fig. 1). $\theta_i = \cos^{-1}(\hat{\mathbf{r}}_{ij} \cdot \hat{\mathbf{u}}_i)$ and $\theta_j = \cos^{-1}(\hat{\mathbf{r}}_{ji} \cdot \hat{\mathbf{u}}_j)$ are the angles between $\hat{\mathbf{r}}_{ij}$ and patches i and j , respectively. $\hat{\mathbf{u}}_i$ and $\hat{\mathbf{u}}_j$ are the vectors normal to the faces upon which patches i and j sit (Fig. 1). σ_{ang} determines how quickly the potential decays with any deviation from perfect alignment and is set at 0.2 in this work.¹⁶ The embedded interaction sites with angular attenuation are similar to a

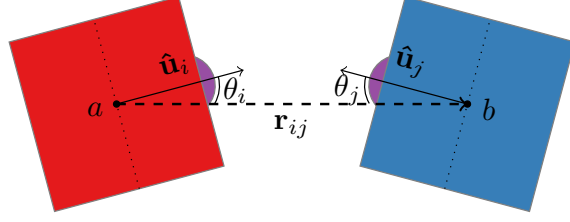


Figure 1: Schematic representation of the interaction between patches i and j on two cubes a and b , showing the definition of the angles θ_i and θ_j .

previous model for patchy spherical particles.^{35–37}

Each patch is also given an intrinsic orientation, pointing from the center of the face to which the patch belongs to the center of one of the face’s edges. The torsional attenuation of the interaction between two patches depends on the torsional angle between their orientation vectors, with the Gaussian form

$$V^{\text{tor}}(\mathbf{r}_{ij}, \hat{\mathbf{v}}_i, \hat{\mathbf{v}}_j) = \exp\left(\frac{-\varphi_{ij}^2}{2\sigma_{\text{tor}}^2}\right), \quad (3)$$

where φ_{ij} is the torsional angle between the two orientation vectors ($\hat{\mathbf{v}}_i$ and $\hat{\mathbf{v}}_j$) of patches i and j . The width of the Gaussian, σ_{tor} , controls how quickly the potential is attenuated as the torsional angle rotates from 0, and is set here to 0.7.

The overall form of the potential is therefore

$$V_{ij}^{\text{patch}}(\mathbf{r}_{ij}, \hat{\mathbf{u}}_i, \hat{\mathbf{u}}_j) = \left[\frac{V_{ij}^{\text{M}}(r_{ij}) - V_{ij}^{\text{M}}(2d)}{\varepsilon_{ij} - V_{ij}^{\text{M}}(2d)} \right] \Theta(2d - r_{ij}) V^{\text{ang}}(\hat{\mathbf{r}}_{ij}, \hat{\mathbf{u}}_i, \hat{\mathbf{u}}_j) V^{\text{tor}}(\mathbf{r}_{ij}, \hat{\mathbf{v}}_i, \hat{\mathbf{v}}_j), \quad (4)$$

where $\mathbf{r}_{ij} = r_{ij}\hat{\mathbf{r}}_{ij}$ and Θ is the Heaviside step function, which enforces the cut-off at $r_{ij} = 2d$.

The total interaction energy between any two particles is given by

$$V_{ab}^{\text{cube}}(\mathbf{r}_{ab}, \boldsymbol{\Omega}_a, \boldsymbol{\Omega}_b) = \sum_{i \in a} \sum_{j \in b} V_{ij}^{\text{patch}}(\mathbf{r}_{ij}, \hat{\mathbf{u}}_i, \hat{\mathbf{u}}_j) \Delta_{ij}(\hat{\mathbf{r}}_{ij}, \boldsymbol{\Omega}_a, \boldsymbol{\Omega}_b), \quad (5)$$

where $\boldsymbol{\Omega}_a$ represents the orientation of particle a and \mathbf{r}_{ab} is the vector from the center of particle a to the center of particle b . $\Delta_{ij} = 1$ if the faces on which patches i and j sit are

the closest pair of most aligned faces of the two cubes, and 0 otherwise. Δ_{ij} therefore acts as an angular truncation of the potential. The strength of the interaction is negligible at the point of truncation (typically less than $10^{-6}\varepsilon_{ij}$).

Dynamical Monte Carlo algorithm

Dynamical simulations of the patchy cube model are performed using our hybrid MC algorithm, which combines bulk diffusion moves with internal relaxation moves to produce trajectories with correct relative diffusion rates for clusters of different sizes as well as collective internal motion. The algorithm is specifically designed to cope with the inhomogeneous structure of a self-assembling system and has been described in full previously.¹⁶ Here we summarize its key features.

Diffusion moves act on entire isolated clusters, defined as collections of particles connected by non-zero energetic interactions. One such cluster is uniformly chosen to be moved. Half of the diffusion moves are translational, and the other half rotational. A translational diffusion move is constructed by picking a random displacement on a Gaussian distribution in each dimension. For a rotational move, a similar approach is used to generate random rotation vectors about the cluster’s center of mass.³⁸ The magnitudes of translations and rotations are scaled to account for two factors. First, under Brownian motion, the translational and rotational diffusion constants of spherical particles depend on the radius of the sphere. For this purpose, our clusters are approximated as spheres with radius proportional to $n^{1/3}$ where n is the number of particles in the cluster. Second, the size of moves is scaled to ensure that the quotient of translational to rotational diffusion respects the Stokes–Einstein relations.

The internal relaxation of clusters is handled with the symmetrized Virtual Move Monte Carlo (VMMC) algorithm.^{39,40} VMMC begins by picking a seed particle and then recruits neighboring particles for the proposed translation or rotation according to the change in potential energy incurred. This approach therefore effectively accounts for forces through the approximate gradient of the potential.

In all simulations we will use a reduced temperature T^* , defined as

$$T^* = k_{\text{B}}T/\varepsilon, \quad (6)$$

where ε is the mean minimum interaction energy between all pairs of patches in the target structure, $\langle \varepsilon_{ij} \rangle_{i,j}$.

The reduced temperature is also used to define a relative time scale for our simulations. The dynamical algorithm described in this section provides control over the diffusion rates of aggregates in the simulation. The rate of diffusion is determined by the width of the distribution from which moves are selected, which we fix at $0.2d$, giving a good acceptance of the internal relaxation moves across a wide range of temperatures. However, Stokes–Einstein diffusion constants are proportional to temperature, and so we must consider the reduced temperature when defining the reduced time. The reduced relative time is taken as

$$t^* = s/T^*, \quad (7)$$

where s is the number of MC sweeps completed and a sweep in an N -particle system consists of N MC trial moves.

Quantifying Fragment Competition

Completeness Index

In order to assess the state of a system in the process of assembling into multiple copies of a target structure, we introduce a completeness index, which identifies competition between fragments that may prevent a system from reaching maximum yield. The analysis can be applied to any instance of addressable assembly, *i.e.*, where each particle in the target structure is unique and so appears exactly once per copy.

The algorithm identifies all aggregates present in a given configuration (defined by non-

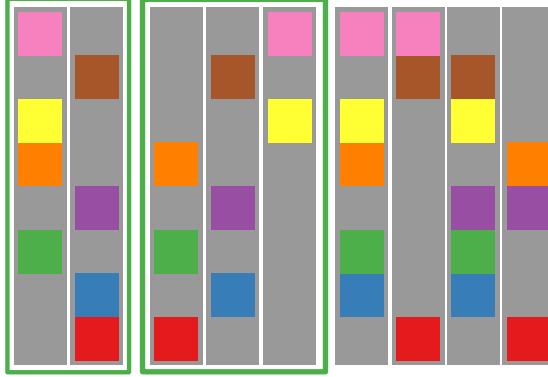


Figure 2: An example of the completability algorithm for a cluster of eight unique components, identified here by color. There are four copies of each component, enough to make a maximum of four complete clusters. At a given instant the building-blocks may have assembled into multiple fragments, indicated in this example by vertical gray bars. The job of the completability algorithm is to determine the maximum number of complete targets (involving one component of each color) that can be formed by the fragments, which in this case is two, as indicated by the green boxes. No further targets or larger aggregates may be made from the remaining fragments because they have overlapping compositions.

zero energetic interactions between the building-blocks), and determines the maximum number of complete target clusters that can be formed by combining them. An example of the task is shown in Fig. 2, where there are enough particles to build four target structures, but the existing fragments can only be combined to complete two of them. The task is a combinatorics problem that can be expressed in the formalism of linear programming (LP). An LP problem is a constrained optimization problem where the objective function is linear and the constraints are linear equalities or inequalities. LP problems take the general form

$$\begin{aligned}
 & \text{maximize} && \mathbf{c}^T \mathbf{x} \\
 & \text{subject to} && \mathbf{A} \mathbf{x} \leq \mathbf{b} \\
 & && \text{and } \mathbf{x} \geq \mathbf{0}.
 \end{aligned} \tag{8}$$

Here, \mathbf{x} is a variable vector of length m whose components are to be optimized in order to find the constrained maximum value of $\mathbf{c}^T \mathbf{x}$. The vectors \mathbf{c} and \mathbf{b} are of length m and n respectively and their values are both fixed. \mathbf{A} is a given $n \times m$ matrix. The vector \mathbf{c} contains

the coefficients of the variables in the objective function ($\mathbf{c}^T \mathbf{x}$), while \mathbf{A} and \mathbf{b} embody the constraints.

LP is commonly used to solve assignment problems, which typically take the form of assigning N workers to N tasks in the optimal way, given that the performance of different workers on different tasks may vary. In the context of addressable assembly, we express the sorting of fragments from the output of a simulation into the largest possible number of target clusters as a binary LP problem (where the components of the vector \mathbf{x} are all either 1 or 0).

To analyze the completability of a given snapshot from a simulation, we first need to obtain a list of all fragments that it contains, along with their compositions. We must also test whether each of these fragments is valid. A valid cluster is a correctly structured sub-fragment of the target cluster,¹⁶ one requirement of which is that it contains no more than one of each particle type. Any fragments that are not valid must be excluded from the analysis, and the number of possible targets reduced accordingly. For example, if the target cluster consists of four particles $ABCD$, and there are ten copies of each particle in the simulation, but we have identified and discounted the invalid cluster ABA , then it is now only possible to complete a maximum of eight targets, since two A particles have been removed.

Given the set of identified fragments, we solve the following problem. We define a number of sets, equal to the maximum number of possible targets. Each fragment may be placed in a set, taking with it all of its particles. We define the score of a set as the number of particles it contains, and an overall objective function \mathcal{N} as the sum of all set scores, *i.e.*, the total number of particles placed into sets. We then maximize \mathcal{N} by varying the assignment of fragments to sets, subject to the constraints that each fragment may only appear in at most one set, and that each set may only contain at most one of each type of particle. Finally, we define the completability index of the fragments as the ratio of the number of completable sets to the maximum number of targets that could, in principle, be built from the original

monomers. In the example of Fig. 2 only two complete targets can be obtained from the fragments, but there are four copies of each monomer, so the completability is $\frac{1}{2}$.

Algorithm

Here, we show how to formulate the fragment assignment as an LP problem like that in Eq. (8). To omit the formal presentation of the completability algorithm, readers may skip to the Results section at this point.

We start by expressing the fragments in a given configuration as a binary string. For instance, in an eight-component cluster with building-blocks $A-H$, the fragment $ABDF$ would be $(1, 1, 0, 1, 0, 1, 0, 0)$. The sum of the string gives an indication of how complete the fragment is, with only a correct target achieving the maximum value.

Now consider a system of N_r copies of each N_t types of building-blocks, divided into N_f independent fragments. Note that N_r is also the maximum number of targets that can be created simultaneously. Similarly to the fragment strings, the assignment of fragments to sets (combinations of fragments in our proposed solution) may be expressed as a binary vector of length N_f . For example, in a system with four fragments, the set vector $(0, 1, 0, 1)$ would imply that fragments 2 and 4 belong to the set, but that 1 and 3 do not.

The assignment of the N_f fragments into sets may therefore be represented by a concatenation of all the N_r individual set vectors. There are N_r set vectors, as this is the maximum number of possible targets. The assignment vector \mathbf{x} therefore has the form

$$\mathbf{x} = \left(\begin{array}{c} \left(\begin{array}{c} \vdots \end{array} \right) \} \mathbf{s}_1 \\ \left(\begin{array}{c} \vdots \end{array} \right) \} \mathbf{s}_2 \\ \vdots \\ \left(\begin{array}{c} \vdots \end{array} \right) \} \mathbf{s}_{N_r} \end{array} \right), \quad (9)$$

where \mathbf{s}_1 is the first set vector. \mathbf{x} has length $N_f N_r$.

We can collect the scores (sum of the binary strings) of the N_f fragments in a vector,

$$\mathbf{n} = \begin{pmatrix} n_1 \\ n_2 \\ \vdots \\ n_{N_f} \end{pmatrix}, \quad (10)$$

where n_1 is the score of the first fragment. We may also define the vector \mathbf{c} , as N_r repeats of \mathbf{n} ,

$$\mathbf{c} = \begin{pmatrix} \mathbf{n} \\ \mathbf{n} \\ \vdots \\ \mathbf{n} \end{pmatrix}, \quad (11)$$

which has the same length, $N_f N_r$, as \mathbf{x} . The column vectors \mathbf{c} and \mathbf{x} define our objective function, $\mathcal{N} = \mathbf{c}^T \mathbf{x}$, which is equal to the total number of particles placed into sets. The maximum of this function corresponds to all particles being placed into sets, meaning that all N_r target structures are complete. We therefore want to maximize \mathcal{N} subject to two constraints:

1. No fragment appears more than once in \mathbf{x} .
2. No type of building-block appears more than once in any set.

To construct the constraint matrix \mathbf{A} , we first introduce the matrix $\tilde{\mathbf{A}}$ with dimensions $N_t \times N_f$ to encode the compositions of the fragments. Element \tilde{A}_{ij} of $\tilde{\mathbf{A}}$ is 1 if fragment j contains building-block type i , and 0 if not. The constraint matrix is then given in block

form by N_r copies of $\tilde{\mathbf{A}}$ and N_r copies of the $N_f \times N_f$ identity matrix \mathbf{I} in the arrangement,

$$\mathbf{A} = \begin{pmatrix} \tilde{\mathbf{A}} & & & \\ & \tilde{\mathbf{A}} & & \\ & & \ddots & \\ & & & \tilde{\mathbf{A}} \\ \mathbf{I} & \mathbf{I} & \dots & \mathbf{I} \end{pmatrix}. \quad (12)$$

\mathbf{A} therefore has dimensions $(N_r N_t + N_f) \times N_f N_r$ and the product $\mathbf{A}\mathbf{x}$ has $N_r N_t + N_f$ elements. The first $N_r N_t$ elements of $\mathbf{A}\mathbf{x}$ give the number of building-blocks of each type in each set, starting with the number of A blocks in set 1, the number of B blocks in set 1, *etc.*, then moving onto the number of each type in set 2, *etc.* The remaining N_f elements of $\mathbf{A}\mathbf{x}$ give the number of times each fragment has been assigned to any set, in the order fragment 1, fragment 2, *etc.*

The two constraints are fulfilled so long as every element of $\mathbf{A}\mathbf{x}$ is less than or equal to 1. Considering the first inequality in Eq. (8), it follows that the constraint vector \mathbf{b} is simply a vector of length $(N_r N_t + N_f)$ where every element is equal to 1. We now have the definitions of the vectors and matrices required by Eq. (8) (\mathbf{c} , \mathbf{x} , \mathbf{b} and \mathbf{A}) in order to optimize $\mathcal{N} = \mathbf{c}^T \mathbf{x}$. Maximization of this function will sort fragments into sets in such a way as to complete as many copies of the target structure as possible. The number of complete targets can then be determined by inspecting the elements of \mathbf{x} after optimization.

If an invalid fragment arises, then the total number of targets that can be formed is now less than the number of replicas of each building-block type. In such a case, using the formalism presented here, the value of N_r must be reduced appropriately, which in turn reduces the number of sets to be created in the vector \mathbf{x} .

The global maximum of the objective function \mathcal{N} may not be unique. If \mathcal{N} takes its largest possible value of $N_r N_t$ then any multiple solutions simply correspond to different ways of combining the fragments to create complete targets. However, when it is not possible to

resolve the system into a full contingent of completed targets, a set of degenerate maxima may exist. While some maxima may correspond to the largest number of completed targets, others may correspond to a larger number of incomplete sets, such that the same number of particles placed into sets overall is the same. To ensure that the maximum number of targets has been found, we use the following procedure. If a full contingent of targets is not found then an attempt is made to build one more than was found previously. This is done by reducing the size of the matrices to include a smaller number of fragment sets. If a solution exists with this reduced number of complete targets, then the algorithm is forced to find it because any incomplete sets would decrease the overall score. The number of targets is then incremented by one again, and the test is repeated. When it is not possible to build the incremented number of targets, the number actually found is the true maximum. Therefore this guarantees that the maximum number of targets is found, provided that the algorithm used to solve the binary LP problem does indeed return a global maximum.

A detailed example of the completability algorithm, including the explicit form of the matrix equations, is given in the Supporting Information as an illustrative case.

Results

We will use two test clusters to investigate the impact of target geometry, connectivity and bond-strength heterogeneity on self-assembly. The idealized (lowest-energy) geometry of the clusters is shown in Fig. 3. Both clusters are comprised of twenty particles, each of which is unique. Target A (Fig. 3 top) is a compact $5 \times 2 \times 2$ cuboid of particles. In contrast, target B (Fig. 3 bottom) has an open, cage-like structure, resembling a $3 \times 3 \times 3$ cube with the face- and body-center particles absent. In the first instance, the adjacent faces of all neighboring particles interact equally and specifically, *i.e.*, $\varepsilon_{ij} = \varepsilon$ for faces that are in contact in Fig. 3 and $\varepsilon_{ij} = 0$ otherwise, thereby encoding addressability into the building-blocks.

Each self-assembly data-point presented here is the mean of 25 dynamical MC simula-

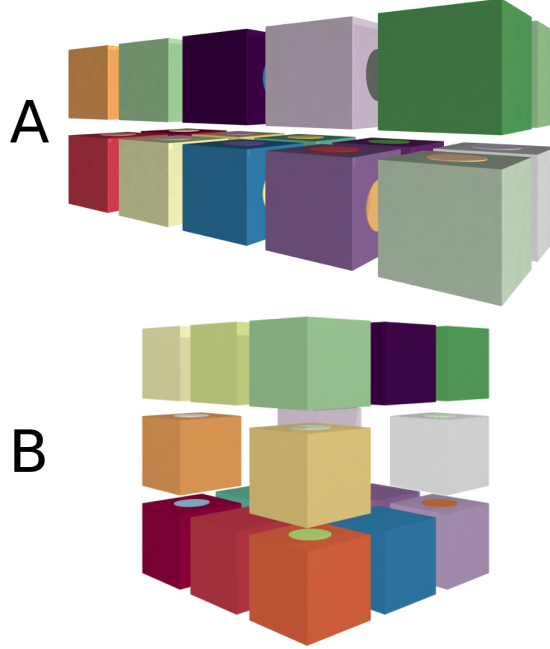


Figure 3: The two target clusters used in this work, both consisting of twenty unique particles: a compact structure A (top), and an open cage structure B (bottom).

tions at each set of conditions. Each simulation begins from a distinct starting configuration consisting of a disordered fluid of monomers, generated from a single high-temperature simulation. Self-assembly is initiated by an instantaneous quench to the assembly temperature of interest. In all simulations, each component is present at a number density of $0.002d^{-3}$. All the simulations contain 80 particles, enough to make a total of 4 targets. Simulating multiple replicas of each component is essential to observe fragment competition, which many simulation studies of addressable assembly have neglected. Even so, we note that any study of self-assembly in a finite system with a fixed number of particles cannot capture all relevant density fluctuations.⁴¹ The standardized conditions of the simulations described here facilitate comparisons within this limitation.

Target clusters

The yields of both target clusters after an assembly time of $t^* = 1.33 \times 10^8$ are shown as a function of the assembly temperature in Fig. 4. This time gives the building-blocks a

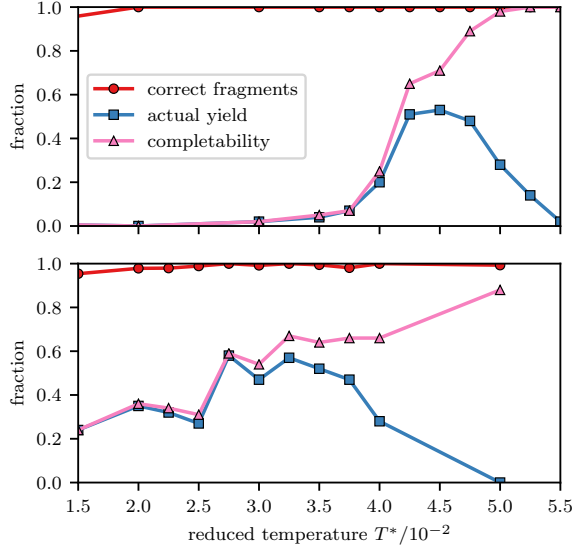


Figure 4: The yields of complete targets and correct partial fragments, and the completability index for target A (top) and target B (bottom).

chance to respond to the assembly temperature and allows us to monitor kinetic progress even though assembly may continue beyond this point of observation. In these plots, the mean yield, which is the fraction of particles in complete and correct clusters, is shown by the blue squares. The pink triangles show the mean completability index of the fragments present at the end of the simulation, and indicate the frustration present in the system due to fragments with mutually incompatible compositions. Such fragments must break up before their building-blocks can be combined into complete targets. The red circles indicate the fraction of particles in correct fragments, *i.e.*, complete targets and sub-fragments of that target in which all particles are in the correct positions and mutual orientations.

For target A (Fig. 4 top) optimal assembly occurs within a narrow temperature window, $T^* \approx [4.25, 4.5] \times 10^{-2}$. Above this temperature range the cluster is thermodynamically unstable, and the system exists mainly as small aggregates and monomers. This is discernible from the combination of low actual yield but high completability in Fig. 4. At temperatures below optimal, this cluster suffers from severe frustration, which limits the extent of assembly possible. The close pairing of the yield and completability lines shows that assembly has proceeded as far as possible with the existing fragments, and that some fragments must first

break up for further progress to be made. Incomplete fragments become increasingly stable at low temperatures, making frustration harder to correct and effectively capping the maximum yield at very low values. Yields at optimal temperatures are modest at approximately 50%, and lie below the maximum completability. This implies that assembly has become slow for this structure, and that there may be steric effects that stall assembly as fragments near completion.

The equivalent plot for target B has a different character, showing a completability index that decays much more gradually with decreasing temperature. Yields in the optimal range of $T^* \approx [2.75, 3.75] \times 10^{-2}$ are similar to those for target A. For both targets, the fraction of particles in correct fragments is always high, showing that self-assembly is not inhibited by erroneous binding or uncontrolled growth of fragments.

Bonding topology

These preliminary results show that frustration between incompatible fragments is a significant factor in limiting the self-assembly of these target clusters. We will now explore the origin of the problem and demonstrate that it is strongly affected by the characteristics of the bonding network.

The sparsest possible bond network that still connects the cluster is a linear chain that may need to be branched but contains no loops. The advantage of such arrangements is that they make it impossible for the system to aggregate into incompatible clusters, provided that there are equal numbers of each component. However, the addition of just one more link introduces a loop and allows frustrated clusters to arise. For example, consider a target composed of four components A – D arranged in a square, and a system containing eight particles, enough to form two complete targets. The particles might be arranged into the aggregates ABC , AB , CD , D . In the case where the cluster is linearly connected, the only bonding interactions are A – B , B – C and C – D . We may combine clusters ABC with D and AB with CD to form two complete targets. This is the only way to combine these fragments

and any set of valid fragments of this system can always be combined. On the other hand, if the cluster has a looped connectivity, where A and D may also bind, we would also have the possibility to combine clusters AB and D , to produce DAB , ABC and CD . This configuration is frustrated, as the fragments present cannot be combined to create any targets without first breaking into smaller clusters.

Two new connectivities of target A were designed, one linear, and one featuring a single loop. These connectivities are shown in Fig. 5 A1 and A2, where blue spheres represent the location of particles, and red lines the links between them. The yield plots for these connectivities are presented in Fig. 6. For the linearly connected structure, the fraction of correct fragments and the completability index remain at 1 across the entire temperature range simulated. This confirms that fragments are assembling without error and that there is never any incompatibility or frustration between fragments. Nevertheless, it can take time for fragments to meet and bind. At the end of the assembly simulations, yield is uniformly high at about 80% except at high temperatures, where any system becomes thermodynamically unstable with respect to dissociation. Note that, due to removing many links, the temperatures at which the target is stable are much lower than for the fully connected cluster A0 (Fig. 4, top). The shift is a potentially important consideration in practice, since a self-assembled nano-structure or material may be required to operate at a particular temperature in a given application.

Since the linear bonding scheme contains the smallest number of bonds necessary to hold the target together, a single break would split the cluster. It is therefore tempting at least to close the chain of bonds into a single loop, which can be done by adding one bond to give scheme A2 in Fig. 5. The addition of this bond has a dramatic and detrimental effect on assembly, as shown in the lower panel of Fig. 6. First, yield at all temperatures closely follows the completability index, indicating that further progress is limited by competition between incompatible fragments. Secondly, the fraction of correct fragments has dropped to about 80% across most of the temperature range. The incorrect fragments consist of chains

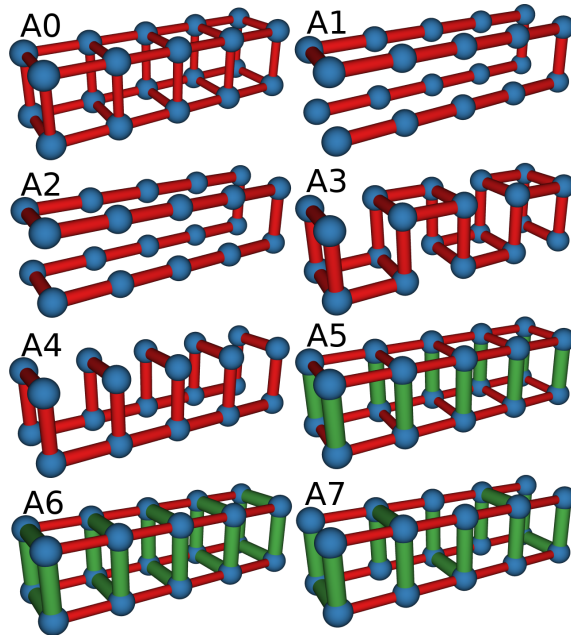


Figure 5: Bonding schemes for variations on target A simulated in this work. A1 and A2 are the linear and looped connectivities respectively. A3 contains loops of four particles and A4 contains loops of eight. Schemes A5–A7 contain a mixture of stronger (green) and weaker (red) bonds. In A5, the strong bonds define disconnected dimers, while in A6 and A7 they define looped and linear tetramers, respectively.

where individual bonds are approximately correct, but the structure has failed to close up overall, leading to a spiral that continues to grow, as illustrated in Fig. 7. This is also a consequence of the loop in the bonding scheme, since growth is automatically terminated at the ends of the chain in the linear bonding scheme.

The likelihood of a structure like A2 failing to close depends on the flexibility of the individual links, which determines the floppiness of the structure as a whole. The formation of incorrect fragments therefore depends on the details of the building-blocks and their bonding, and is a separate obstacle to self-assembly from the competition between correct fragments. Although the linear bonding scheme A1 prevents run-away growth and leads to high yields, the final structure is still floppy. Hence, an entirely linear bonding scheme may still not be satisfactory in practice, especially for larger structures.

The fully connected bonding scheme A0 of target A effectively contains a very large number of loops but assembles more effectively than the singly-looped scheme A2. Fig. 5

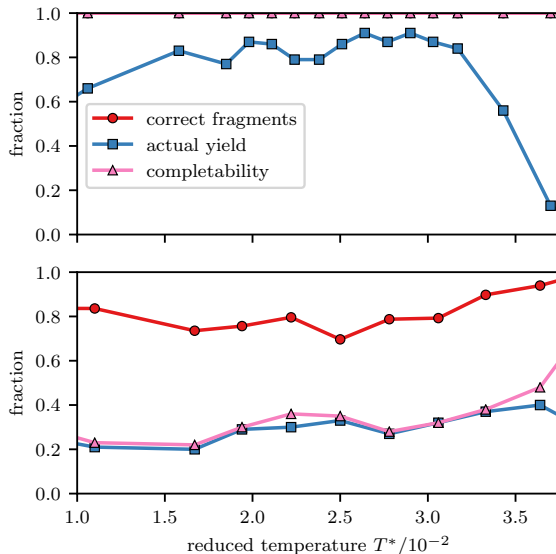


Figure 6: Yield, completability and fraction of correct fragments for the linearly connected A1 (top) and single-loop A2 (bottom) bonding schemes of target A.

shows two possible intermediate connectivities that lie between the extremes of A0 and A2. Scheme A3 contains multiple loops of four particles, while A4 has multiple loops of eight particles. The results of self-assembly for A3 and A4 are shown in Fig. 8. The smaller loops in both these schemes are both successful in eliminating the incorrect structures that appeared for scheme A2. The scheme with the smallest loops, A3, is also successful at alleviating fragment competition compared to A2. However, neither of these intermediate schemes reaches peak yields as high as the fully-connected scheme A0. Any benefit from limiting the possible combinations of competing fragments in the intermediate schemes is outweighed by the fact that the particles only have a coordination number of 2 or 3 (compared to 3 or 4 in scheme A0). The lower temperatures required for assembly of A3 and A4 therefore intensify the competition between incompatible fragments.

Heterogeneous bond energies

Altering the topology of the bonding network as in schemes A1–A4 amounts to switching edges on and off in the graph of neighboring building-blocks so that ε_{ij} takes one of only two values: ε or 0. Finer control can be exerted by altering the strength of individual bonds.

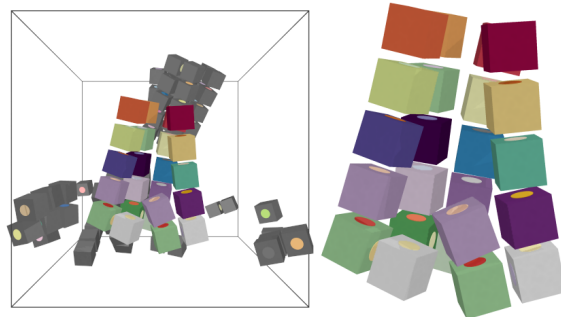


Figure 7: Left: A simulation snapshot of target A2 (with a single loop of bonds connecting particles in the target geometry). An incorrect aggregate is highlighted in the center of the simulation box, where the flexibility of the structure has allowed the aggregate to grow rather than closing the loop and terminating assembly. Right: An isolated view of the erroneous cluster.

In DNA-based systems, this is readily achieved through the choice of the nucleotides or the length of the complementary sequences.²⁰

From previous work, we know that using different bond strengths can promote hierarchical assembly pathways, since fragments where the monomers are connected by strong links are more likely to persist long enough to encounter and bind to each other than weakly bound ones.¹⁶ Having assembled to an intermediate stage, the interactions between fragments are boosted if they can interact over multiple sites in their larger combined interfaces, thereby driving the next stage of assembly. Hierarchical assembly is normally envisaged in the case where the structure itself is modular and symmetrical.⁴² However, such an approach is not advantageous in all cases.^{16,43} Because of the uniqueness of building-blocks for fully addressable targets, they have no formal modularity, but a hierarchical path could nevertheless be used to limit the scope for fragment competition by controlling the fragments that are likely to arise.

This principle is demonstrated by the bonding network A5, illustrated in Fig. 5, where target A has been divided into 10 strongly-bound dimers that are linked to each other by weaker bonds. There can be no competition in the pairing of building-blocks into addressable dimers, so promoting early formation of these fragments effectively reduces the number of unique components for assembly of the full target from 20 to 10.

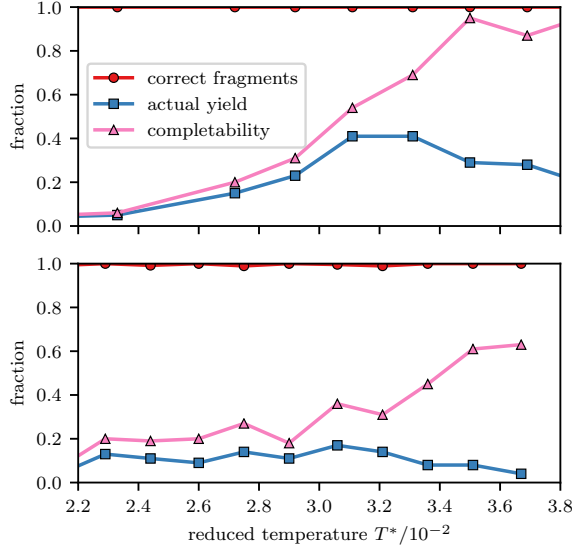


Figure 8: Yield, completability and fraction of correct fragments for bonding schemes A3 (top) and A4 (bottom) with intermediate connectivity (illustrated in Fig. 5).

The performance of model A5 is shown in Fig. 9 for a range of ratios of bond strengths (keeping the total binding energy of the cluster fixed for comparison). The results for the homogeneous bond scheme A0 (Fig. 4) are shown as faint lines for comparison. We see that dramatic improvement is possible with the inhomogeneous bond scheme. Fragment competition is indeed alleviated, as revealed by the higher completability index at lower temperatures, especially for bonding-strength ratios above 1.5. This has the effect of suppressing kinetic trapping due to fragment competition, thereby broadening the temperature range for successful assembly at the lower end and allowing higher peak yields (up to 80%) to be reached at the end of the chosen assembly time. It is only at strong:weak ratios of about 3 that some of the high-temperature performance starts to be lost, due to the weaker bonds then being insufficient to stabilize the overall structure.

Another possible hierarchical scheme for target A would be to divide it into five slices, each of which is a square tetramer defined by strong bonds, linked to each other by weaker bonds. The tetramers may be cyclically connected, as in scheme A6 of Fig. 5, or linearly connected (omitting one edge of each square), as in scheme A7. The performance of both schemes is shown in Fig. 10, again comparing with the heterogeneous scheme A0 from Fig. 4.

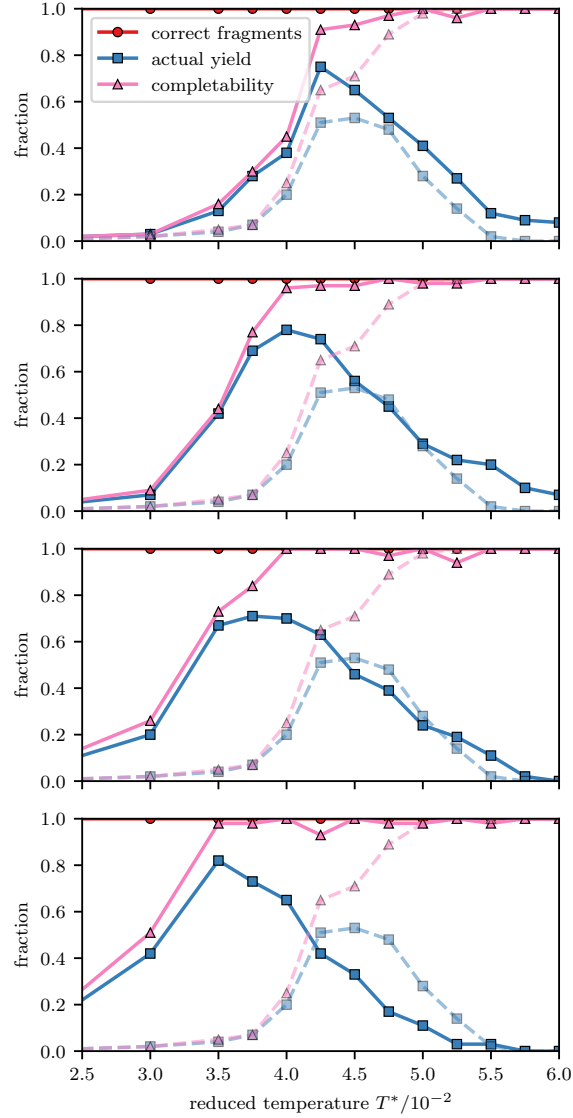


Figure 9: Yield, completability and fraction of correct fragments for bonding scheme A5, where target A has been divided into strongly-bound dimers. From top to bottom the panels refer to strong:weak binding strength ratios of 1.5, 2, 2.5 and 3. The faint dashed lines show the results for bonds of equal strength (Fig. 4).

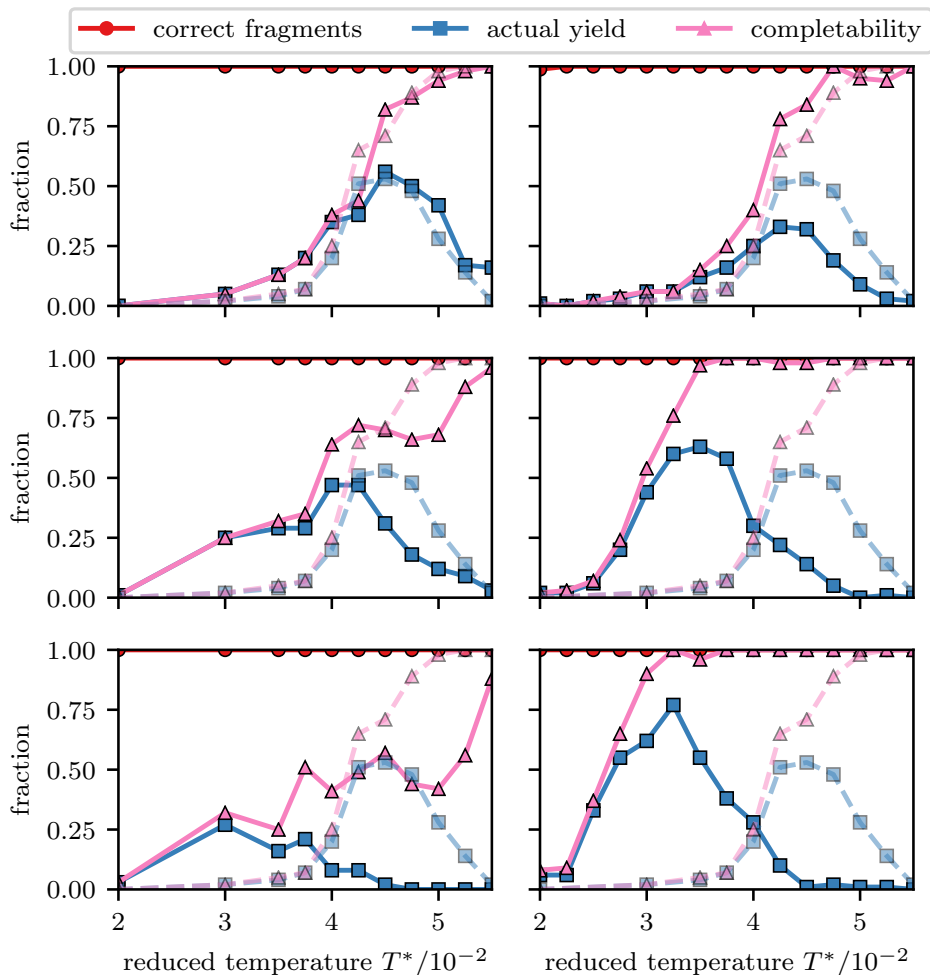


Figure 10: Yield, completability and fraction of correct fragments for bonding schemes A6 (left) and A7 (right), where target A has been divided into strongly-bound tetramers that are cyclically (A6) or linearly (A7) linked. From top to bottom, the panels refer to strong:weak binding strength ratios of 1.5, 2.5 and 3. The faint dashed lines show the results for bonds of equal strength (Fig. 4).

The cyclic tetramer scheme A6 has modest success in broadening the temperature range of assembly for bond-strength ratios around 2–2.5, but peak yield is not improved. The scheme suffers from fragment competition in the first stage of assembly, due to the cycle of bonds in the tetramers, thereby stalling the second stage. The linearly bonded tetramer scheme A7 is much more effective, since fragment competition is avoided at both stages of assembly, provided that the stages are energetically well separated. At sufficiently low

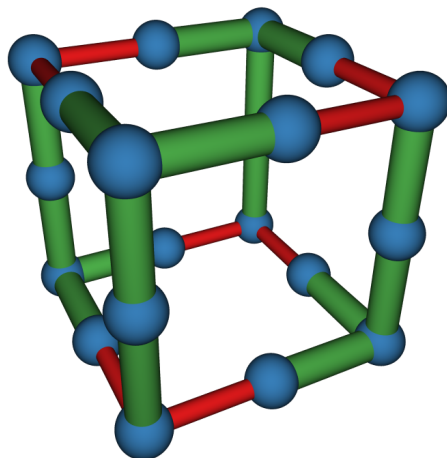


Figure 11: Heterogeneous bonding scheme B1 for target B, dividing the structure into four pentamers. Green and red cylinders indicate strong and weak links, respectively.

temperature, fragment competition does return because even fragments bound by the weaker links then become long-lived and impede formation of the tetramers. Overall, peak yields approach those of the dimer scheme A5, but with a slightly narrower range of assembly temperatures.

A hierarchical scheme can also be used to improve the self-assembly of the more open target B. On the basis of the results so far, we expect the most successful scheme to omit bonding loops at least in the first stage of assembly. A symmetrical scheme of heterogeneous bonding is shown in Fig. 11. The graph of bonds in the strongly-linked pentamer fragments is now branched but still non-cyclic, thereby avoiding the possibility of fragment competition in formation of the first-stage fragments. Yield curves for this scheme are presented in Fig. 12. As predicted, the hierarchical scheme with non-cyclic fragments suffers less from fragment competition at low temperatures than the homogeneously bonded scheme. The peak yield is over 90% at the optimum temperature for a bond-strength ratio of 3. For this target, assembly temperatures are shifted noticeably downwards in the heterogeneous scheme because the structure must still be held together by a relatively small number of weak links.

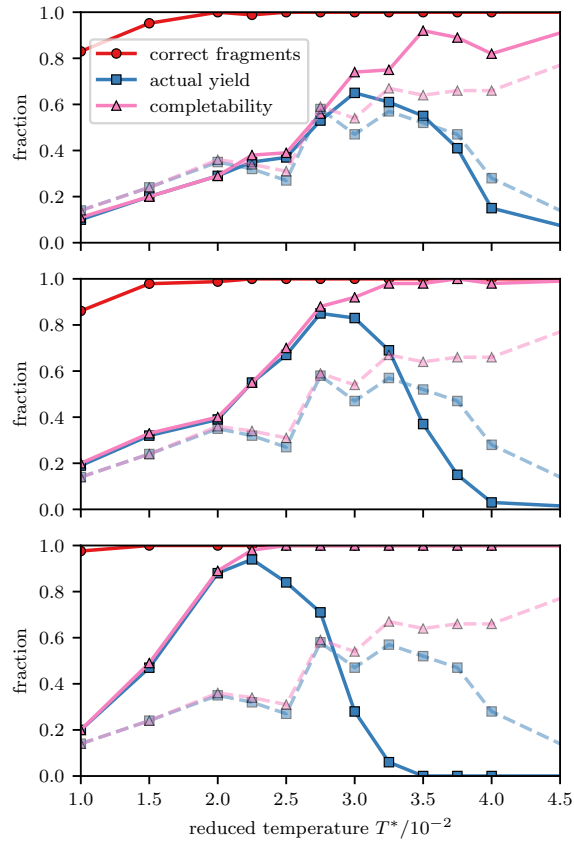


Figure 12: Yield, completability and fraction of correct fragments for the heterogeneous bonding scheme of target B1 illustrated in Fig. 11. From top to bottom, the panels refer to strong:weak binding strength ratios of 1.5, 2 and 3. The faint dashed lines the results for the homogeneous bond scheme (Fig. 4).

Randomized schemes

The placements of strong and weak links in schemes A5, A7 and B1 were guided by our observation that linear connectivities avoid competition between fragments and that competition is particularly undesirable in the early stages of assembly. To test whether this intuitive approach is strictly necessary, we have briefly examined schemes where a given number of strong bonds are distributed randomly in a fully connected network of bonds for target A. The procedure is described in more detail in the Supporting Information and the results are shown in Fig. S1. The main effect of the randomly placed strong bonds is to shift the assembly temperature downwards slightly. For a small-to-intermediate number of strong bonds, there can be a small increase in peak yield and a slight widening of the temperature range for successful assembly. However, the full advantages of a strategically chosen network are not realized by random placement.

Bond strengths do not have to be restricted to two values and, in some applications such as DNA bricks, naturally have a continuous distribution about their mean. Theoretical and computational work by Jacobs *et al.*²¹ has predicted that a spread of bond energies can assist addressable assembly by stabilizing small, floppy structures and lowering the nucleation barrier for assembly. We have tested Gaussian distributions of bond strengths with a selection of different widths for target A, as described in more detail in the supporting material. For this modest-sized target structure and the choice of assembly protocol used in the present work, we found little effect of random bond-strength heterogeneity (Fig. S2). Any slight alleviation of fragment competition was accompanied by a slight loss of peak yield.

Conclusions

The aim of any self-assembly process is to produce the maximum number of complete, defect-free target structures in a reasonable time. In this work, we have examined one of the

ubiquitous potential obstacles to this goal, which is the formation of, and frustration between multiple incomplete fragments. This possibility is particularly pertinent in the context of addressable assembly, where only specific combinations of building-blocks are permitted. In contrast to the majority of computational studies of addressable assembly, we have explicitly included competition between multiple copies of the target structure in our simulations.

We have quantified the incompatibility of fragments at a given stage of assembly by introducing a completability index, which determines the globally optimal way of combining fragments. It is important to realize that this index is not a static quantity and is likely to change nonmonotonically over the course of self-assembly. If assembly is initialized from disconnected monomers, the completability begins at unity. Similarly, if all components are successfully incorporated into defect-free targets then the completability ends at unity. However, the completability index drops when it detects intermediate fragments that cannot be combined in principle, due to their incompatible compositions. This competition may slow down assembly because some fragments must break up before progress can be made. Depending on the severity of the competition, it may also limit the final yield of the target that can be achieved in practice, even if no erroneous structures have formed. In this work, we have compared all schemes after a fixed assembly time. This provides a way to judge the efficiency of assembly, even though different schemes may be advancing at somewhat different rates at any given cut-off time.¹⁶

An important general result that the completability index makes clear is that fragment competition is ruled out in any system where the network of bonds contains no cycles. In such cases, correctly formed fragments can never be incompatible with completion of the maximum number of targets due to their composition alone. In practice, other considerations also come into play. Depending on the nature of the binding, cycle-free designs are likely to be too floppy. Except at very low temperature, they are also vulnerable to dissociation because every edge is a cut-edge in the graph of bonds; hence, disruption of any bond breaks the structure. Floppiness can also lead to incorrect fragments due to uncontrolled growth.

In the present work, such growth is one of the few causes of invalid aggregation because we have taken the selectivity of building-block interactions to be perfect. In the presence of cross-interactions, aggregation is an additional obstacle to self-assembly.²⁹

Building on these observations, we have shown that a successful strategy for efficient assembly is to encourage partially hierarchical assembly pathways in which the first steps involve formation of cycle-free fragments. If the stages of assembly can be cleanly separated then this approach effectively reduces the complexity of the later stages to assembly of a smaller number of addressable fragments. As previous work¹⁶ and the contrasting targets A and B in this contribution show, the best choice of stepwise path depends on the specific target, including steric considerations. We note that very recent experimental developments now make it possible to follow the assembly of addressable structures of the size we have considered here and to manipulate pathways by selectively altering bond strengths.²⁰

In this work, the assembly protocol has been an instantaneous quench from a low-density dispersion of monomers at high temperature to a range of fixed assembly temperatures. This has allowed us to judge the success of self-assembly not only by the peak yield after a given time, but also by the range of temperatures over which assembly is successful even if sub-optimal. Robustness with respect to the precise conditions is a desirable property of a practical self-assembling system, since performance is then less dependent on fine-tuning. Addressable assembly of DNA bricks can indeed operate successfully by incubation at fixed temperature,¹³ although a gradually decreasing temperature ramp¹⁴ can have the advantage of encouraging nucleation at a small number of sites at high temperature, followed by growth to completion at a lower temperature.^{21,22} We note that a time-dependent protocol could be used to enhance the partly hierarchical approach suggested here, since it would allow a greater separation of energy scales to come into play in succession, thereby avoiding interference between the different stages of assembly. With such an approach, the results of this work could be used to control fragment competition at each scale in the proposed ensemble of pathways.

Supporting Information Available

The following files are available free of charge.

Self-assembly results for randomly placed strong bonds (Figure S1); Self-assembly results for a Gaussian distribution of bond energies (Figure S2); worked example of completability algorithm.

References

- (1) Pawar, A. B.; Kretzschmar, I. Fabrication, assembly, and application of patchy particles. *Macromol. Rapid Commun.* **2010**, *31*, 150–168.
- (2) Yi, G.; Pine, D. J.; Sacanna, S. Recent progress on patchy colloids and their self-assembly. *J. Phys.: Condens. Matter* **2013**, *25*, 193101.
- (3) Wang, Y.; Wang, Y.; Breed, D. R.; Manoharan, V. N.; Feng, L.; Hollingsworth, A. D.; Weck, M.; Pine, D. J. Colloids with valence and specific directional bonding. *Nature* **2012**, *491*, 51–55.
- (4) Jones, M. R.; Seeman, N. C.; Mirkin, C. A. Programmable materials and the nature of the DNA bond. *Science* **2015**, *347*, 1260901.
- (5) Alivisatos, A. P.; Johnsson, K. P.; Peng, X.; Wilson, T. E.; Loweth, C. J.; Bruchez, M. P.; Schultz, P. G. Organization of ‘nanocrystal molecules’ using DNA. *Nature* **1996**, *382*, 609–611.
- (6) Mirkin, C. A.; Letsinger, R. L.; Mucic, R. C.; Storhoff, J. J. A DNA-based method for rationally assembling nanoparticles into macroscopic materials. *Nature* **1996**, *382*, 607–609.
- (7) Liu, W.; Halverson, J.; Tian, Y.; Tkachenko, A. V.; Gang, O. Self-organized architectures from assorted DNA-framed nanoparticles. *Nature Chem.* **2016**, *8*, 867–873.

- (8) Rothemund, P. W. K. Folding DNA to create nanoscale shapes and patterns. *Nature* **2006**, *440*, 297–302.
- (9) Hong, F.; Zhang, F.; Liu, Y.; Yan, H. DNA Origami: Scaffolds for creating higher order structures. *Chem. Rev.* **2017**, *117*, 12584–12640.
- (10) Wei, B.; Dai, M.; Yin, P. Complex shapes self-assembled from single-stranded DNA tiles. *Nature* **2012**, *485*, 623–626.
- (11) Tikhomirov, G.; Petersen, P.; Qian, L. Fractal assembly of micrometre-scale DNA origami arrays with arbitrary patterns. *Nature* **2017**, *552*, 67–71.
- (12) Ke, Y.; Ong, L. L.; Shih, W. M.; Yin, P. Three-dimensional structures self-assembled from DNA bricks. *Science* **2012**, *338*, 1177–1183.
- (13) Ke, Y.; Ong, L. L.; Sun, W.; Song, J.; Dong, M.; Shih, W. M.; Yin, P. DNA brick crystals with prescribed depths. *Nature Chem.* **2014**, *6*, 994–1002.
- (14) Ong, L. L.; Hanikel, N.; Yaghi, O. K.; Grun, C.; Strauss, M. T.; Bron, P.; Lai-Kee-Him, J.; Scheuder, F.; Wang, B.; Wang, P. et al. Programmable self-assembly of three-dimensional nanostructures from 10,000 unique components. *Nature* **2017**, *552*, 72–77.
- (15) Frenkel, D. Order through entropy. *Nature Mater.* **2015**, *14*, 9–12.
- (16) Madge, J.; Miller, M. A. Design strategies for self-assembly of discrete targets. *J. Chem. Phys.* **2015**, *143*, 044905.
- (17) Johnson, J. E.; Speir, J. A. Quasi-equivalent viruses: a paradigm for protein assemblies. *J. Mol. Biol.* **1997**, *269*, 665–675.
- (18) Cademartiri, L.; Bishop, K. J. M. Programmable self-assembly. *Nature Mater.* **2015**, *14*, 2–9.

- (19) Reinhardt, A.; Frenkel, D. Numerical Evidence for Nucleated Self-Assembly of DNA Brick Structures. *Phys. Rev. Lett.* **2014**, *112*, 238103.
- (20) Sajfutdinow, M.; Jacobs, W. M.; Reinhardt, A.; Schneider, C.; Smith, D. M. Direct observation and rational design of nucleation behavior in addressable self-assembly. *Proc. Nat. Acad. Sci. USA* **2018**, *115*, E5877–E5886.
- (21) Jacobs, W. M.; Reinhardt, A.; Frenkel, D. Rational design of self-assembly pathways for complex multicomponent structures. *Proc. Nat. Acad. Sci. USA* **2015**, *112*, 6313–6318.
- (22) Jacobs, W. M.; Reinhardt, A.; Frenkel, D. Communication: Theoretical prediction of free-energy landscapes for complex self-assembly. *J. Chem. Phys.* **2015**, *142*, 021101.
- (23) Jacobs, W. M.; Frenkel, D. Self-assembly of structures with addressable complexity. *J. Am. Chem. Soc.* **2016**, *138*, 2457–2467.
- (24) Fullerton, C. J.; Jack, R. L. Optimising self-assembly through time-dependent interactions. *J. Chem. Phys.* **2016**, *145*, 244505.
- (25) Wales, D. J. Atomic clusters with addressable complexity. *J. Chem. Phys.* **2017**, *146*, 054406.
- (26) Fejer, S. N.; Mantell, R. G.; Wales, D. J. Designing hierarchical molecular complexity: icosahedra of addressable icosahedra. *Mol. Phys.* **2018**, *116*, 2954–2964.
- (27) Halverson, J. D.; Tkachenko, A. V. DNA-programmed mesoscopic architecture. *Phys. Rev. E* **2013**, *87*, 062310.
- (28) Halverson, J. D.; Tkachenko, A. V. Programmable self-assembly of thin-shell mesostructures. *J. Chem. Phys.* **2017**, *147*, 141103.
- (29) Madge, J.; Miller, M. A. Optimising minimal building blocks for addressable self-assembly. *Soft Matter* **2017**, *13*, 7780–7792.

- (30) Jacobs, W. M.; Oxtoby, D. W.; Frenkel, D. Phase separation in solutions with specific and nonspecific interactions. *J. Chem. Phys.* **2014**, *140*, 204109.
- (31) Gottschalk, S.; Lin, M. C.; Manocha, D. *Proceedings of ACM Siggraph*; Association for Computing Machinery: New York, 1996; pp 171–180.
- (32) Smallenburg, F.; Filion, L.; Marechal, M.; Dijkstra, M. Vacancy-stabilized crystalline order in hard cubes. *Proc. Nat. Acad. Sci. USA* **2012**, *109*, 17886–17890.
- (33) John, B. S.; Escobedo, F. A. Phase behavior of colloidal hard tetragonal parallelepipeds (cuboids): A Monte Carlo simulation study. *J. Phys. Chem. B* **2005**, *109*, 23008–23015.
- (34) Wilber, A. W.; Doye, J. P. K.; Louis, A. A.; Lewis, A. C. F. Monodisperse self-assembly in a model with protein-like interactions. *J. Chem. Phys.* **2009**, *131*, 175102.
- (35) Doye, J. P. K.; Louis, A. A.; Lin, I.; Allen, L. R.; Noya, E. G.; Wilber, A. W.; Kok, H. C.; Lyus, R. Controlling crystallization and its absence: proteins, colloids and patchy models. *Phys. Chem. Chem. Phys.* **2007**, *9*, 2197–2205.
- (36) Villar, G.; Wilber, A. W.; Williamson, A. J.; Thiara, P.; Doye, J. P. K.; Louis, A. A.; Jochum, M. N.; Lewis, A. C. F.; Levy, E. D. Self-assembly and evolution of homomeric protein complexes. *Phys. Rev. Lett.* **2009**, *102*, 118106.
- (37) Wilber, A. W.; Doye, J. P. K.; Louis, A. A. Self-assembly of monodisperse clusters: Dependence on target geometry. *J. Chem. Phys.* **2009**, *131*, 175101.
- (38) Romano, F.; Michele, C. D.; Marenduzzo, D.; Sanz, E. Monte Carlo and event-driven dynamics of Brownian particles with orientational degrees of freedom. *J. Chem. Phys.* **2011**, *135*, 124106.
- (39) Whitlam, S.; Geissler, P. L. Avoiding unphysical kinetic traps in Monte Carlo simulations of strongly attractive particles. *J. Chem. Phys.* **2007**, *127*, 154101.

- (40) Whitelam, S.; Feng, E. H.; Hagan, M. F.; Geissler, P. L. The role of collective motion in examples of coarsening and self-assembly. *Soft Matter* **2009**, *5*, 1251–1262.
- (41) Ouldridge, T. E.; Louis, A. A.; Doye, J. P. K. Extracting bulk properties of self-assembling systems from small simulations. *J. Phys.: Condens. Matter* **2010**, *22*, 104102.
- (42) Gröschel, A. H.; Walther, A.; Löbbling, T. I.; Schacher, F. H.; Schmalz, H.; Müller, A. H. E. Guided hierarchical co-assembly of soft patchy nanoparticles. *Nature* **2013**, *503*, 247–251.
- (43) Haxton, T. K.; Whitelam, S. Do hierarchical structures assemble best via hierarchical pathways? *Soft Matter* **2013**, *9*, 6851–6861.